Antarctic volcanoes: A remote but significant hazard

A. Geyer [(1)], A. Martí [(2)], S. Giralt [(1)], A. Folch[(2)]

Institute of Earth Sciences Jaume Almera (ICTJA-CSIC), Lluis Solé i Sabaris s/n, 08028 Barcelona, Spain
Barcelona Supercomputing Center (BSC), Jordi Girona 29, 08034 Barcelona, Spain

EGU2017-6667

POSVOLDEC

1. Introduction and objectives

- Ash emitted during explosive volcanic eruptions may disperse over vast areas of the globe posing a threat to human health and infrastructures and causing enormous disruption to air traffic.
- In Antarctica, no attention has been paid to the potential socio-economic and environmental consequences of an ash-forming eruption occurring at high southern latitudes.
- We show here how **ash from Antarctic volcanoes may pose a threat higher than previously believed**, volcanic ash could potentially encircle the globe, leading to significant consequences to global aviation safety.

2. Antarctic Volcanoes

From the tens of volcanoes located in Antarctica, at least nine are known to be active and five of them, all stratovolcanoes, **have reported frequent volcanic activity in historical times** (Fig. 1)(Global Volcanism Program, http://www.volcano.si.edu).

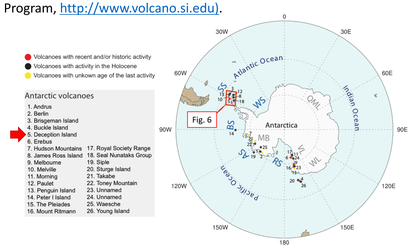

Fig. 1: Location of Antarctic volcanoes listed in Table S1.1. AS: Amundsen Sea; BS: Bellinghausen Sea; MB: Marie Byrd Land; RS: Ross Sea; VL: Victoria Land; WS: Weddell Sea; WL: Wilkes Land.

Mount Erebus.
Photo: British Antarctic Survey

1967 Eruption at Deception Island.
Photo: British Antarctic Survey

3. Methodology

NMMB-MONARCH-ASH model

- NMMB-MONARCH-ASH[1] is a novel on-line meteorological and atmospheric transport model to simulate the emission, transport and deposition of tephra (ash) particles released from volcanic eruptions.
- The **model predicts ash cloud trajectories, concentration at relevant flight levels, and deposit thickness** for both regional and global domains (Table 1).

Table 1. NMMB-MONARCH-ASH model configurations.

NMMB-MONARCH-ASH CONFIGURATION		
	Global Run	**Regional Run**
Dynamics	NMMB (180s time-step)	NMMB (10s time-step)
Physics	Ferrier microphysics BMJ cumulus scheme MYJ PBL scheme LISS land surface model	
Aerosols	5 ash bins	
Source Term (emissions)		
Run duration	9 days	
Eruption duration	12 h	
Vertical distribution	Point source	
MER formulation	Degrayter and Bonadonna (2012)[7]	
Sedimentation model	Ganser (1993)[7]	
Run	**Global Set-up**	**Regional Set-up**
Number of processors	512	256
Domain	Global	Regional
Horizontal resolution	1° x 0.75°	0.052° x 0.037°
Vertical layers	60	
Top of the atmosphere	21 hPa	
Meteorology Boundary Conditions (spatial resolutions)	ECMWF EraInterim Reanalysis (0.75° x 0.75°)	

Eruptive Scenario: 1970 eruption on Deception Island

Deception Island-DI (Fig. 2)[2,3]:

- Composite volcanic system truncated by the formation of a collapse caldera.
- Over 30 post-caldera Holocene eruptions.
- Unrest episodes recorded in 1992, 1999 and 2014-2015.
- Recent explosive eruptions (1967, 1969 and 1970), destroyed or severely damaged the scientific bases operating on the island.

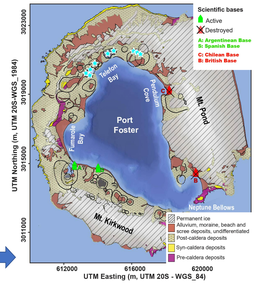

Fig. 2: Simplified geological map of DI [4,5]. Blue stars show the sites of the 1970 volcanic event. Black solid and dashed lines delimit visible and inferred post-caldera volcanic craters.

1967 Eruption at Deception Island
Photo by the Chilean Navy, 1967

1970 Eruption, model source parameters:

- Column height = 10 km
- Deposit volume = 0.1 km^3
- The particle Total Grain Size Distribution (TGSD) reconstructed from tephra deposits measured at neighboring islands and discretized in 5 bins ranging from 2Φ (0.5 mm) to 7Φ (8μm) with a linear dependency of particle density on diameter ranging from 1650 to 2800 kg/m^3.

4. Results

4. 1 Meteorological conditions

A persistent large-scale clock-wise circulation around an upper-level low-pressure zone located close to the Pole is clearly visible at any time.

The polar vortex extends up to the stratosphere, with a global-scale circulation covering latitudes from 70° up to 50° depending on the period.

At these stratospheric levels, the resulting polar jet stream is very intense (wind speeds > 60 m/s), widening notably during the winter (Fig. 3b) and narrowing during the summer (Fig. 3a).

At mid-tropospheric levels, the meteorological situations are characterized by a breaking of the jet stream and a pronunciation of the meanders reaching much lower latitudes.

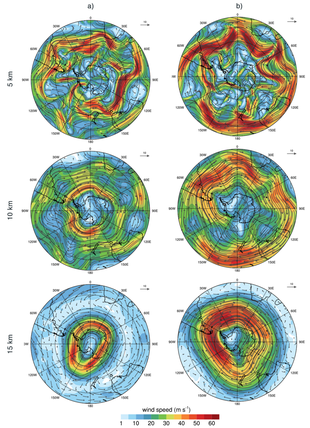

Fig. 3: NMMB-MONARC-ASH meteorological results over the South Pole during the summer (a), and winter (b) seasons. Plots show wind vectors and velocity contours (in ms^{-1}) at 5 (top), 10 (middle) and 15 (bottom) km a.s.l., roughly corresponding to mid-troposphere, tropopause and stratosphere respectively.

4.2 Long-range ash dispersal

Highest cloud column mass load values (>100 g/m^2) are limited to the first 48 h after the eruption start (Fig. 4a).

Residual small amount of ash (0.1-1 g/m^2) is still present in the atmosphere up to 8 days after the eruption onset (Fig. 4a).

Ash concentrations above the flight safety thresholds (0.2-2 mg/m^3) can be observed over South Africa, southern Australia or even over austral Patagonia.

Some ash clouds re-enter back to the Antarctic Continent. However, in most cases, ash clouds circulate around (latitudes 70°-50°) and away (<50°) the continent, i.e. leaving no substantial fallout record on the main land.

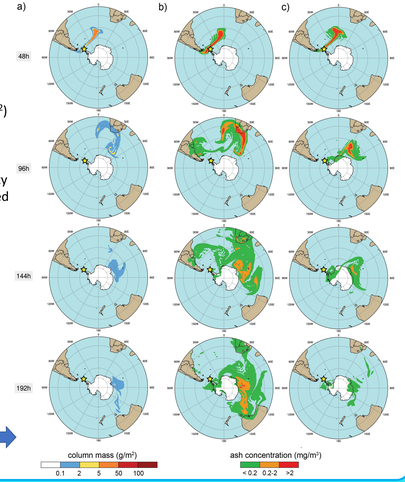

Fig. 4: a) Total column mass loading (in g/m^2), b) the concentration of ash at Flight Level FL050 (in mg/m^3), and c) the concentration at FL250. Safe ash concentration thresholds are shown (red concentration contours illustrate "No Flying" zones). The yellow star indicates the location of Deception Island.

4.3 Ash fallout

The precise orientations or the deposit axes depend on the regional winds during the selected days (Fig. 5).

Deposits exceeding 1 cm in thickness can be found at distances as far as James Ross Island (> 190 km) or beyond Joinville Island (> 230 km).

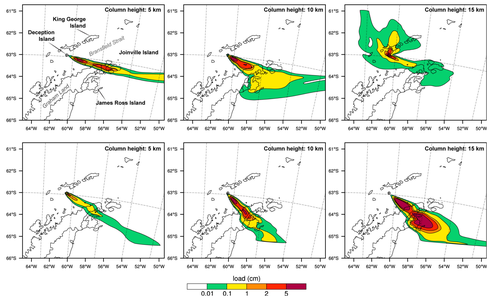

Fig. 5: Ground deposit thickness (in cm) for the 1970-like scenario with different column heights of: 5km (left), 10km (middle), and 15km (right). Top and bottom panels show the corresponding ash deposition for the summer and winter periods, respectively

5. Discussion and implications

Ash from lower-latitude Antarctic volcanoes are likely to encircle the globe, resulting in significant consequences for global aviation safety.

There is a need to perform a complete hazard assessment for other active Antarctic volcanoes located on West Antarctica and along Victoria Land.

Ash fall out may lead also to important regional problems for the scientific research stations and summer field camps in the area and also to touristic vessels operating in the region.

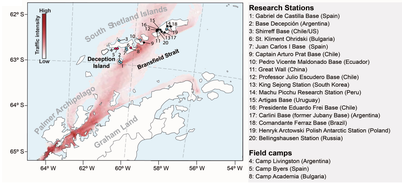

Fig. 6: Location of year-round (black dots) and temporary (only austral summer)(blue dots) research stations nearby Deception Island. Red dots correspond to temporary field camps. The intensity of vessel traffic in the touristic season 2012/13 is also indicated[6]

References

[1] Marti, A., Folch, A., Jorba, O. & Janjic, Z. Volcanic ash modeling with the on-line NMMB/BSC-ASHv1.0 model: model description, case simulation and evaluation. *Atmos. Chem. Phys.* **2017**, 4005-4034, doi: 10.5194/acp-17-4005-2017 (2017).

[2] Roobol, M. J. The volcanic hazard at Deception Island, South Shetland Islands. *British Antarctic Survey Bulletin* **51**, 237-245 (1982).

[3] Bartolini, S., Geyer, A., Martí, J., Pedrazzi, D. & Aguirre-Díaz, G. Volcanic hazard on Deception Island (South Shetland Islands, Antarctica). *Journal of Volcanology and Geothermal Research* **285**, 150-168, doi:10.1016/j.jvolgeores.2014.08.009 (2014).

[4] Smellie, J. L. *et al. Geology and geomorphology of Deception Island*. (Br. Antarct. Surv., Natural Environmental Research Council, 2002).

[5] Martí, J., Geyer, A. & Aguirre-Diaz, G. Origin and evolution of the Deception Island caldera (South Shetland Islands, Antarctica). *Bulletin of Volcanology* **75**, 1-18, doi:10.1007/s00445-013-0732-3 (2013).

[6] Bender, N. A., Crosbie, K. & Lynch, H. J. Patterns of tourism in the Antarctic Peninsula region: a 20-year analysis. *Antarctic Science* **28**, 194-203, doi:10.1017/S0954102016000031 (2016)

Acknowledgements

A.G. thanks the support provided by the Ramón y Cajal research program (RYC-2012-11024). This research was partially funded by the MINECO grants VOLCLIMA (CGL2015-72629-EXP) and POSVOLDEC(CTM2016-79617-P)(AEI/FEDER-UE).